Supplementary Information

Multimeric interacting interface of biologically synthesized zinc oxide nanoparticle corona efficiently sequesters α-synuclein against the protein fibrillation

Running Title: Multimeric functional groups in corona efficiently sequester α-synuclein against the amyloidosis.

Sonali Jena, Kumari Subham, Harshit Kalra, Suman Jha*

Department of Life Science, National Institute of Technology Rourkela, Odisha, 769008, India.

*Corresponding author: Dr. Suman Jha, Department of Life Science, National Institute of Technology Rourkela, Rourkela, 769008, Odisha, India. E-mail address: jhas@nitrkl.ac.in, Tel.: +916612462687.

Index of supporting information contents

Fig. S1: (a) The mean size of zinc oxide nanoparticles with ±SEM was obtained by measuring the diameters of ~ 30 particles from respective TEM micrographs using Image J software, and (b) the colloidal stability of the NPs by measuring the surface potential in phosphate buffer for consecutive five days **Fig. S2:** FTIR spectra of (a) chemically synthesized, (b) tyrosine functionalized and (c) biologically synthesized ZnONPs. **Fig. S3:** EDS analysis of $ZnONP_M$ (Left Panel) HAADF-STEM mapping of $ZnONP_M$, (Right Panel) Table showing elemental composition of $ZnONP_M$. **Table S1:** The phenol and flavonoid content in biologically synthesized ZnONP corona, estimated using tannic acid and quercetin as respective standards. **Fig. S4:** Standard curve of (a) tannic acid, (b) quercetin. **Fig. S5:** Hit spectrum of the phytochemicals obtained from GC-MS analysis of biological synthesized $ZnONP_M$ corona: (a) 3,5-Dimethoxycinnamic acid, (b) Bithionol, (c) 3,7-Dimethoxyflavone, (d) 2,7-Diphenyl-1,6-dioxopyridazino[4,5:2',3']pyrrolo[4',5'-d]pyridazine, (e) S-Nitroso-L-glutathione,(f) Tofisopam, (g) 3,3',7,8-Tetramethoxyflavone. **Table S2:** List of phytochemicals obtained from GC-MS analysis of biologically synthesized $ZnONP_M$ corona. **Fig. S6:** Ligplot results showing the interactions between L-tyrosine and αS. **Fig. S7:** Ligplot results showing interactions of phytochemicals, obtained from GC-MS analysis, (a)3,5-Dimethoxycinnamic acid, (b) 2,7-Diphenyl-1,6-dioxopyridazino [4,5:2',3'] pyrrolo [4',5'd] pyridazine, (c)S-Nitroso-L-glutathione, (d)3,3',7,8-Tetramethoxyflavone with αS protein. **Table S3:** Binding parameters of docked complexes obtained from Ligplot analysis. **Fig. S8:** Aggrescan-based analysis of αS for the potential aggregation-prone area. **Fig. S9:** Time-dependent adsorption of αS onto the ZnONPs interface characterized by (a) Zeta potential of synthesized nanoparticle in phosphate buffer, (b) Neutralization assay, (c) representative HAADF-STEM mapping of αS-ZnONP complexes. **Table S4:** Elemental composition of representative nanoparticle, αS, and nanoparticle-protein agglomerates. **Fig. S10:** (a) SDS-PAGE gel showing the soluble fraction of protein available in the supernatant, (b) intensity plot of the raw gel image. **Fig. S11:** Isotherms showing titration curves when 30 µg/mL (a) chemically synthesized, (b) tyrosine functionalized, and (c) biologically synthesized ZnONPs was titrated with 50 µM αS at 25 °C. **Fig. S12:** Far-UV spectra of 50 µM αS at (a) 0 h and (b) 120 h incubation at 37 °C. **Fig. S13:** Cell viability assay of SH-SY5Y cell upon the treatment of ZnONPs interface using MTT dye reduction assay. SH-SY5Y cells were seeded in a 96-well plate at a density of 10,000 cells/well and allowed to grow overnight. Cells were further treated with increasing concentrations of either the ZnONPs interface (pink-bare NP, yellow-

L-tyrosine functionalized NP, and green-biologically synthesized NP using mango leaf extract) and incubated for 24 h. **Fig. S14:** ROS detection in SH-SY5Y cell upon treatment of different ZnONPs (a) PC (b) $ZnONP_C$, (c) $ZnONP_Y$, (d) $ZnONP_M$, (e) αS M (the protein monomers) using DCFH-DA dye, and (f) Intensity plot from at least 3 images of respective treatments and expressed as arbitrary units (a.u.) calculated using ImageJ software. **Fig. S15**: (a) 10 % SDS PAGE and (b) Relative Intensity (a.u.) plot, for band corresponding to αS (14 kDa) of samples; lane A- Protein Ladder of size 245-11 kDa, lane B- cell lysate, lane C- 50 μM monomeric αS, lane D-soluble fraction of αS available in the flocs, lane E- Supernatant (S1) obtained after centrifugation of nano-formulation complexed cell protein, lane F-solubilized pellet in 1X PBS, lane G-supernatant (S2) obtained after dissolution of the pellet (nano-formulation complexed cell protein), and lane G- $ZnONP_M$. **Table S5**: Concentration of protein calculated by BCA assay.

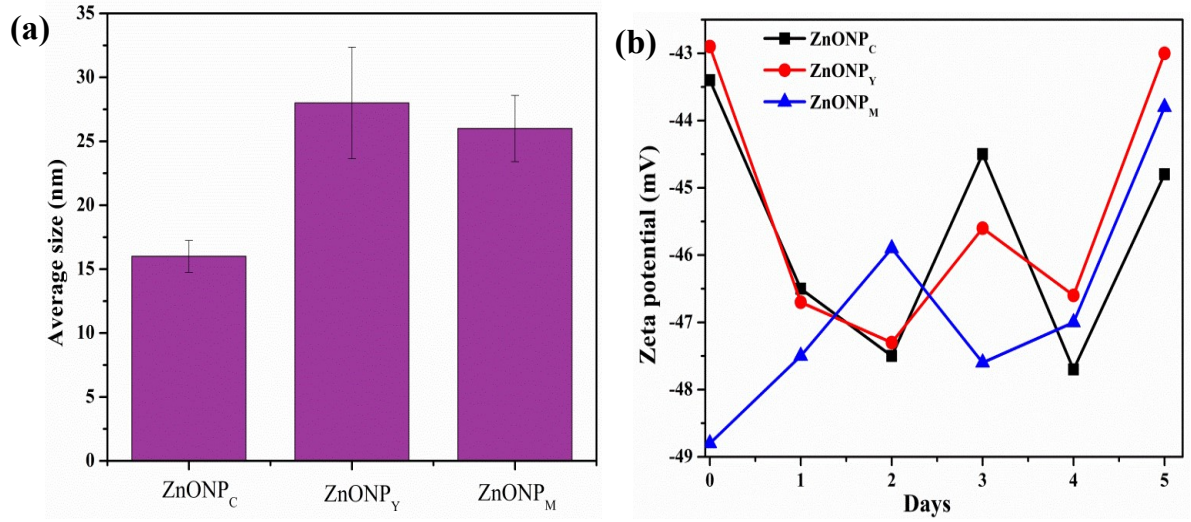

Fig. S1: (a) The mean size of zinc oxide nanoparticles with ±SEM was obtained by measuring the diameters of ~ 30 particles from respective TEM micrographs using Image J software, and (b) the colloidal stability of the NPs by measuring the surface potential in phosphate buffer for consecutive five days.

Methodology: The size distribution of NPs was evaluated using Image J software. Briefly, the average size of at least 30 nanoparticles was obtained from the respective TEM micrographs, and the mean size is plotted as a bar graph with standard error at the mean (±SEM, Fig. S1a). The colloidal stability of all three nanoparticles was checked by measuring the zeta potential over the course of five days. Due to the instrument's technical limitation, i.e. the high ionic strength in the PBS hampered the electric field, hence the quality of the data. Thus, we measured the zeta potential of the nanoparticle in PB instead of PBS. Briefly, the nanoparticles (30 µg/mL) were dissolved in 10 mM PB and incubated at RT for five days and the zeta potential was measured at an interval of 24 h.

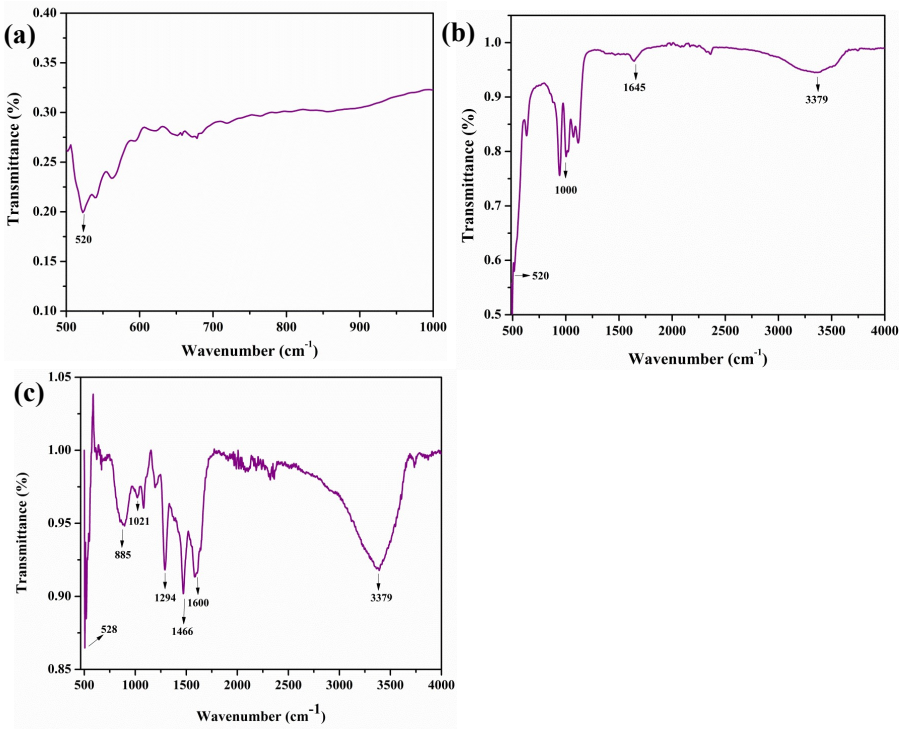

Fig. S2: FTIR spectra of (a) chemically synthesized, (b) tyrosine functionalized and (c) biologically synthesized ZnONPs.

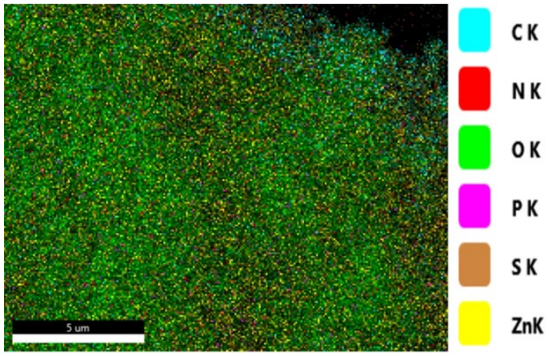

Fig. S3: EDS analysis of $ZnONP_M$ (Left Panel) HAADF-STEM mapping of $ZnONP_M$, (Right Panel) Table showing elemental composition of $ZnONP_M$.

Element	Weight %	Atom %	Net Int.
C K	12.1	31.4	40.8
N K	1.5	3.4	14.9
O K	16.2	31.5	386.4
P K	0.4	0.4	16.7
S K	0.3	0.3	15.9
Zn K	69.5	33.1	274.3

Table S1: The phenol and flavonoid content in biologically synthesized $ZnONP_M$ corona, estimated using tannic acid and quercetin as respective standards.

Samples	Phenol content (µg/mL)	Flavonoid content(µg/mL)
Mango leaf extract	150.95	72.97
$ZnONP_M$	2	8.7

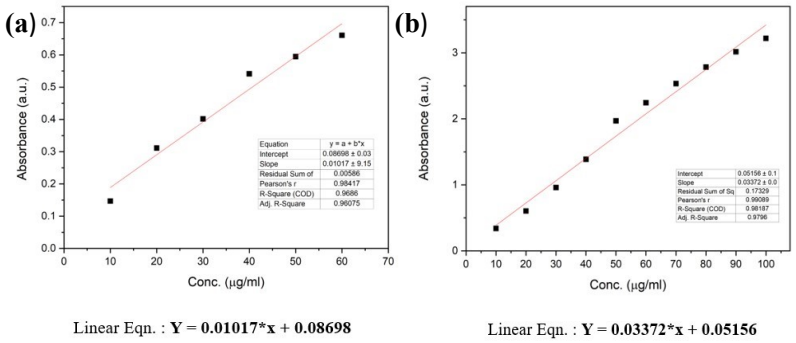

Fig. S4: Standard curve of (a) tannic acid, (b) quercetin.

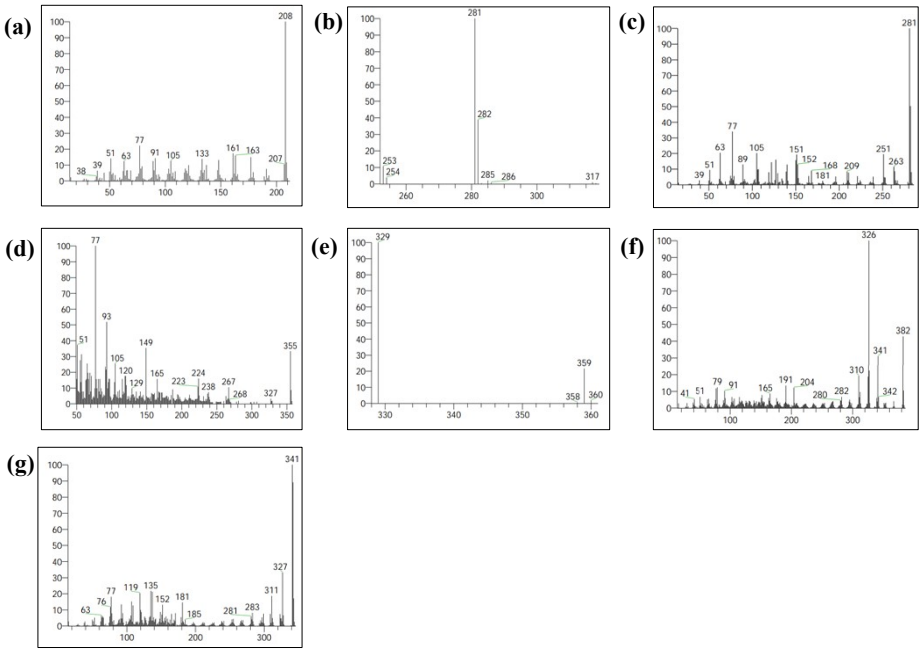

Fig. S5: Hit spectrum of the phytochemicals obtained from GC-MS analysis of biological synthesized $ZnONP_M$ corona: (a) 3,5-Dimethoxycinnamic acid, (b) Bithionol, (c) 3,7-Dimethoxyflavone, (d) 2,7-Diphenyl-1,6-dioxopyridazino[4,5:2',3']pyrrolo[4',5'-d]pyridazine, (e) S-Nitroso-L-glutathione,(f) Tofisopam, (g) 3,3',7,8-Tetramethoxyflavone.

Table S2: GC-MS analysis of plant extract moieties extracted from the corona of biologically synthesized $ZnONP_M$ with its potential biological application(s).

Sl. No.	Retention Time (min)	Compound Name	Mol. Wt. (g/mol)	Biological importance
1	*4.16*	*3,5-Dimethoxycinnamic acid (C11H12O4)*	*208*	• *Prevent αS and prion proteins transformation into amyloid structure.*
2	*5.51*	*Bithionol (C12H6Cl4O2S)*	*354*	• *Inhibitors of Aβ amyloidosis,* • *Protect primary cortical neurons.*
3	*5.55*	*3,7-Dimethoxyflavone (C17H14O4)*	*282*	• *Neuroprotective nature.*
4	*6.49*	*2,7-Diphenyl-1,6-dioxopyridazino[4,5:2',3']pyrrolo[4',5'-d]pyridazine (C20H13N5O2)*	*355*	• *Anti-neurodegenerative,* • *Anti-insomnia,* • *Regulate neurotransmitter release.*
5	*10.81*	*S-Nitroso-L-glutathione* *(C10H16N4O7S)*	*336*	• *Anti-oxidative property,* • *Neuroprotective nature.*
6	*27.05*	*Tofisopam (C22H26N2O4)*	*382*	• *Improves cognitive performance,* • *Enhance attenuated synaptic transmission,* • *Increase glial plasticity.*
7	*32.73*	*3,3',7,8-Tetramethoxyflavone (C19H18O6)*	*342*	• *Anti-oxidative property,* • *Neuroprotective property.*
8	2.91	Trinexapac-ethyl, TMS derivative (C16H24O5Si)	324	NA
9	5.74	2,6-Dihydroxyacetophenone, 2TMS derivative (C14H24O3Si2)	296	• Antibacterial • Anti-oxidative
10	7.53	3,6,2',3'-Tetramethoxyflavone (C19H18O6)	342	• Anti-inflammatory • Anti-oxidative • Anti-cancerous
11	7.53	3,5-	282	• Anti-inflammatory

		Dimethoxyflavone (C17H14O4)		• Anti-oxidative • Anti-cancerous
12	10.70	Propionic acid, 3-[1-(4 methoxyphenyl)-5-thiophen-2-yl-1H-pyrrol -2-yl]- (C18H17NO3S)	327	NA
13	11.08	3-Hydroxy-7,8,2',3'-tetramethoxyflavone (C19H18O7)	358	• Anti-inflammatory • Anti-oxidative • Anti-cancerous
14	16.98	psi.,.psi.-Carotene, 3,4-didehydro-1,2-dihydro-1-methoxy (C41H60O2)	584	• Anti-oxidative
15	17.19	Chromone, 5-hydroxy-6,7,8-trimethoxy-2,3-dimethyl (C14H16O6)	280	• Antibacterial • Anti-oxidative
16	27.36	Phthalic acid, di(2-propylpentyl) ester (C24H38O4)	390	• Antibacterial • Insecticidal
17	28.06	Mono(2-ethylhexyl) phthalate (C16H22O4)	278	• Antibacterial
18	28.15	3',8,8'-Trimethoxy-3-piperidyl-2,2'-binaphthalene1,1',4,4'-tetrone (C28H25NO7)	487	• Anti-cancerous • Anti-oxidative

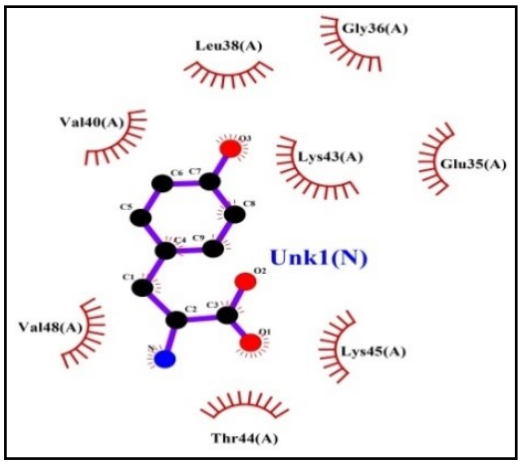

Fig.S6: Ligplot results showing the interactions between L-tyrosine and αS.

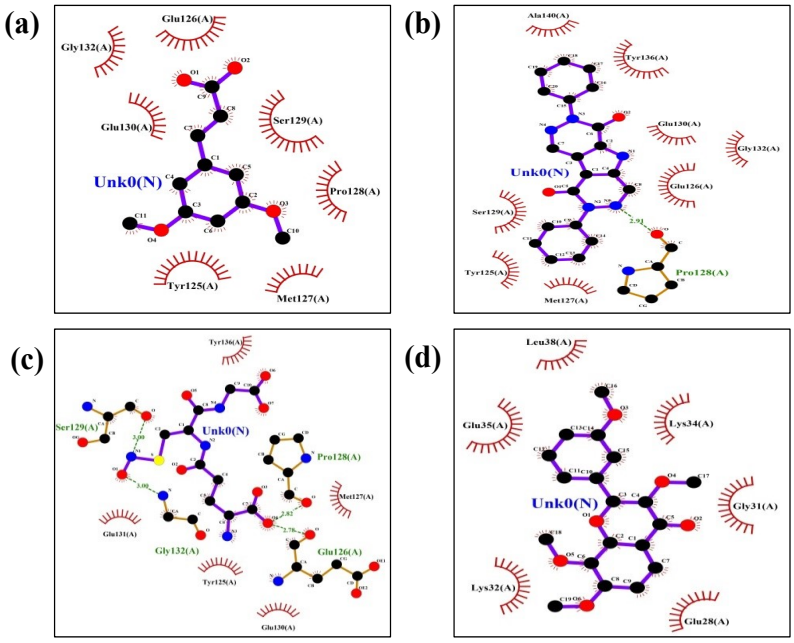

Fig S7: Ligplot results showing interactions of phytochemicals, obtained from GC-MS analysis, (a)3,5-Dimethoxycinnamic acid, (b) 2,7-Diphenyl-1,6-dioxopyridazino [4,5:2',3'] pyrrolo [4',5'd] pyridazine, (c)S-Nitroso-L-glutathione, (d)3,3',7,8-Tetramethoxyflavone with αS protein.

Table S3: Binding parameters of docked complexes obtained from Ligplot analysis.

Sl. No.	Phytochemicals	Interacting amino acids	Mode of interaction	Docking score
4	3,5-Dimethoxycinnamic acid	Tyr125, Glu126, Met127, Pro128, Ser129, Glu130, Gly132	Carbon hydrogen bond, pi-pi stacked, pi-sigma, alkyl bond	-4.5
5	2,7-Diphenyl-1,6-dioxopyridazino [4,5:2',3'] pyrrolo [4',5'd] pyridazine	Glu126, Tyr125, Met127, Ser129, Glu130, Gly132, Tyr136, Ala140	Conventional hydrogen bond	-7.3
6	S-Nitroso-L-glutathione	Tyr125, Glu126, Met127, Pro128, Ser129, Glu130, Glu131, Gly132, Tyr136	Conventional hydrogen bond, unfavorable donor-donor	-3.8
7	3,3',7,8-Tetramethoxyflavone	Glu28, Gly31, Lys32, Lys34, Glu35, Leu38	Carbon-hydrogen bond, alky, pi-alkyl, pi-anion, amide-pi stacked	-5
8	L-tyrosine	Glu35, Gly36, Leu38, Lys43	Carbon-hydrogen bond	-4.5

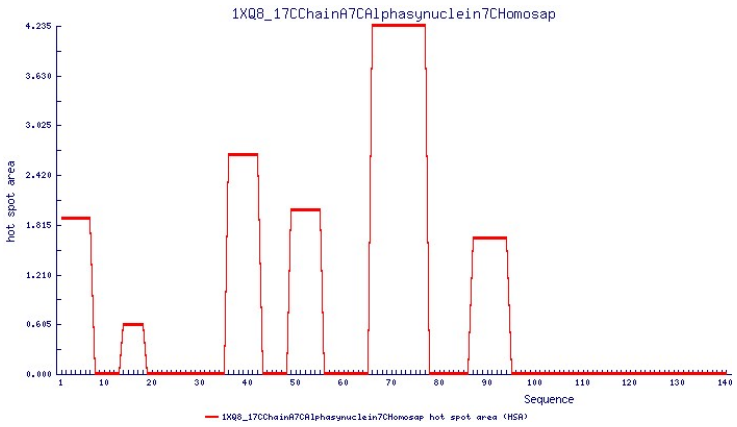

Fig. S8: Aggrescan-based analysis of αS for the potential aggregation-prone area.

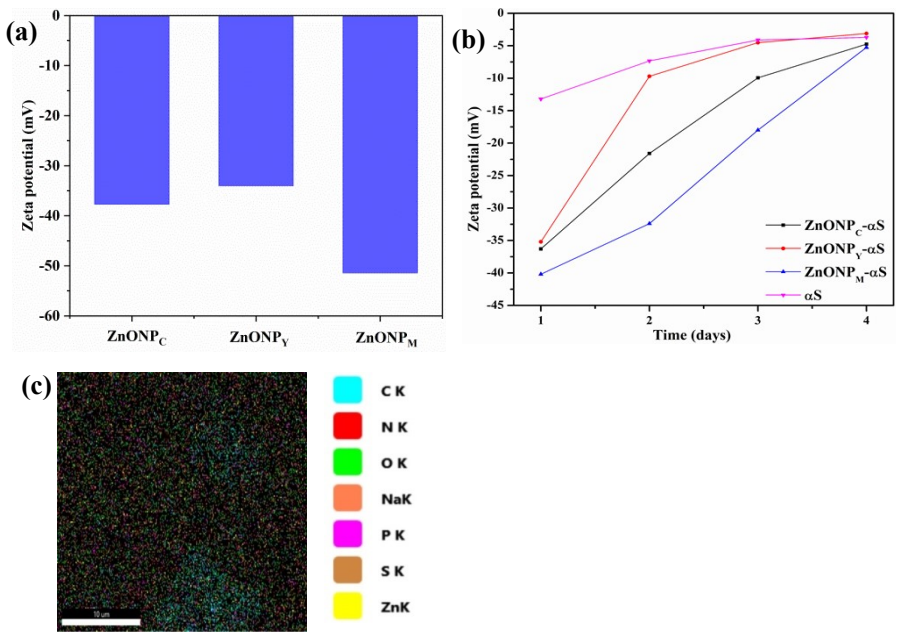

Fig. S9: Time-dependent adsorption of αS onto the ZnONPs interface characterized by (a) Zeta potential of synthesized nanoparticle in phosphate buffer, (b) Neutralization assay, (c) representative HAADF-STEM mapping of αS-ZnONP complexes.

Table S4: Elemental composition of representative nanoparticle, αS, and nanoparticle-protein agglomerates.

Element	**ZnONP**	**αS**	**ZnONP-αS**
C K	NA	13.24	22.68
N K	NA	4.10	6.90
O K	57	82.67	63.28
Zn K	43	NA	7.13

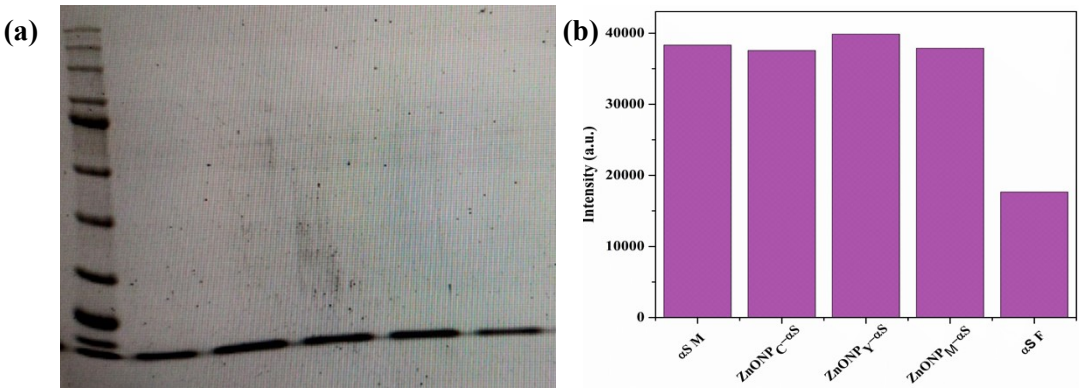

Fig. S10: (a) SDS-PAGE gel showing the soluble fraction of protein available in the supernatant, (b) intensity plot of the raw gel image.

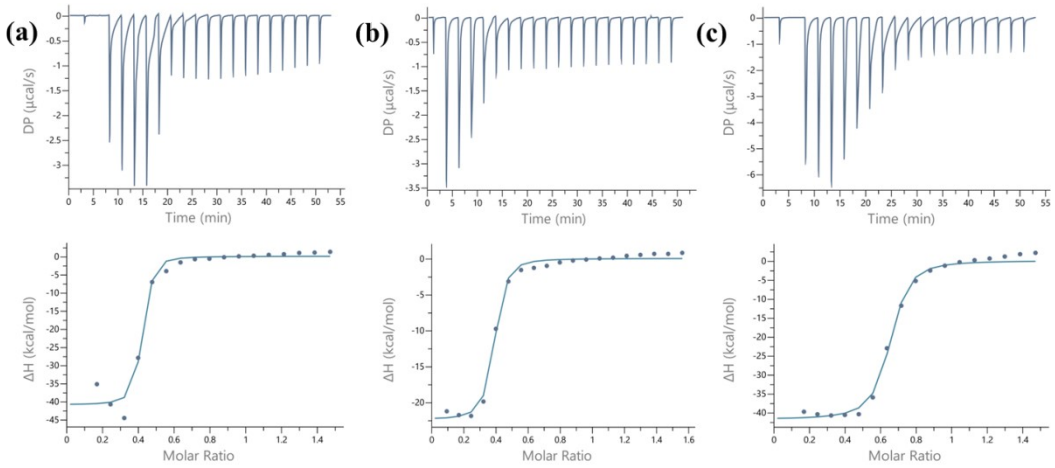

Fig. S11: Isotherms showing titration curves when 30 µg/mL (a) chemically synthesized, (b) tyrosine functionalized, and (c) biologically synthesized ZnONPs was titrated with 50 µM αS at 25 ˚C.

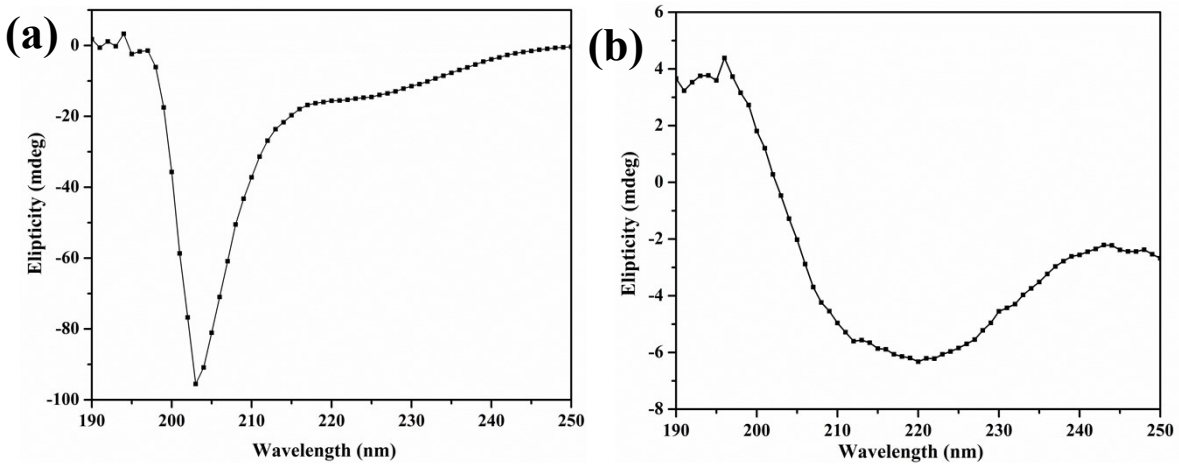

Fig. S12: Far-UV spectra of 50 µM αS at (a) 0 h and (b) 120 h incubation at 37 ºC.

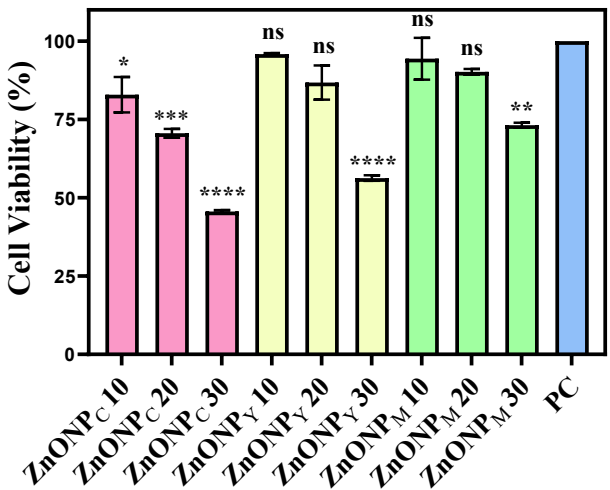

Fig. S13: Cell viability assay of SH-SY5Y cell upon the treatment of ZnONPs interface using MTT dye reduction assay. SH-SY5Y cells were seeded in a 96-well plate at a density of 10,000 cells/well and allowed to grow overnight. Cells were further treated with increasing concentrations of either the ZnONPs interface (pink-bare NP, yellow-L-tyrosine functionalized NP, and green-biologically synthesized NP using mango leaf extract) and incubated for 24 h. Cells without any treatment was taken as control, PC (ns - nonsignificant, * for $P < 0.05$, ** for $P < 0.001$, *** for $P < 0.0003$, **** for $P < 0.0001$ with respect to PC obtained in ordinary one-way ANOVA).

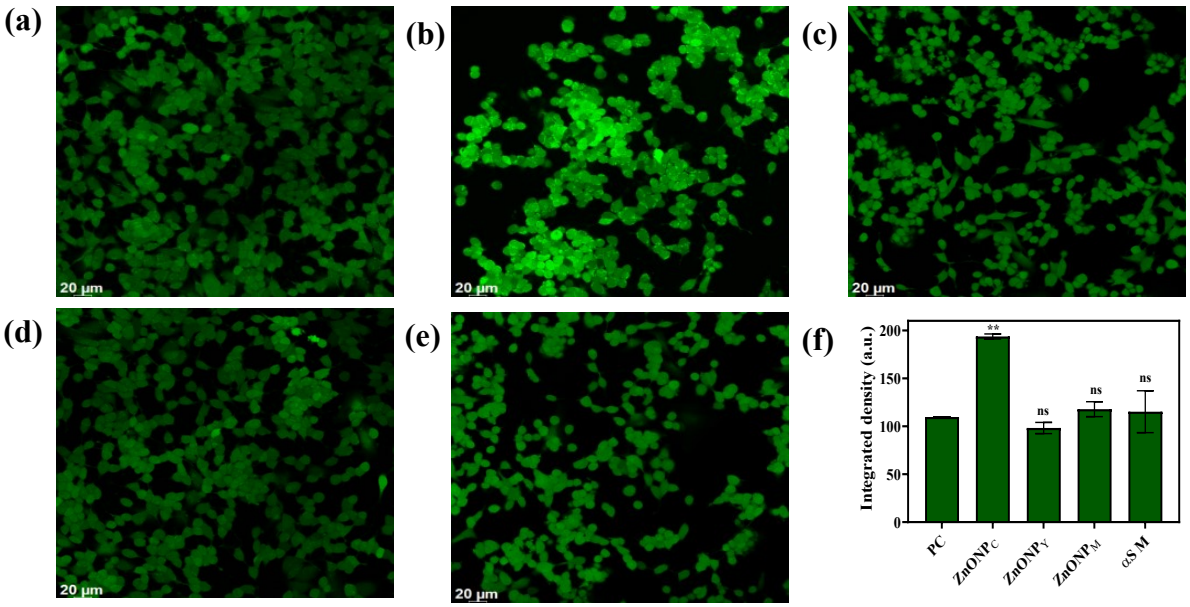

Fig. S14: ROS detection in SH-SY5Y cell upon treatment of different ZnONPs (a) PC (b) $ZnONP_C$, (c) $ZnONP_Y$, (d) $ZnONP_M$, (e) αS M (the protein monomers) using DCFH-DA dye,

and (f) Intensity plot from at least 3 images of respective treatments and expressed as arbitrary units (a.u.) calculated using ImageJ software. Cells without any treatment taken as positive control, PC (ns - nonsignificant, ** for $P < 0.001$, with respect to PC obtained in ordinary one-way ANOVA).

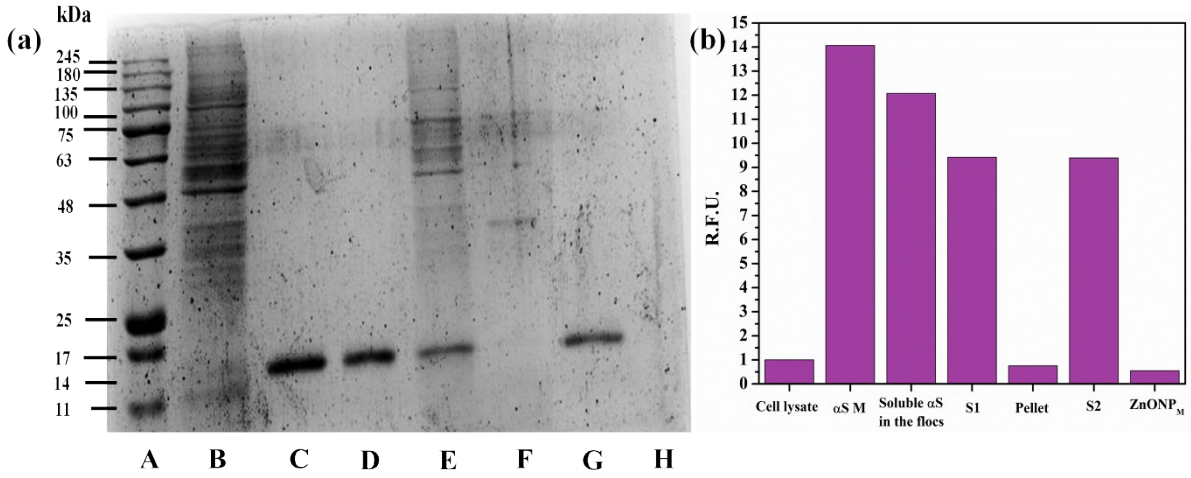

Fig. S15: (a) 10 % SDS PAGE and (b) Relative Intensity (a.u.) plot, for band corresponding to αS (14 kDa) of samples in lane A- Protein Marker of size 245-11 kDa, lane B- cell lysate, lane C- 50 μM monomeric αS, lane D-soluble fraction of αS available in the flocs, lane E- Supernatant (S1) obtained after centrifugation of nano-formulation complexed total cell protein, lane F- solubilized pellet in 1X PBS, lane G-supernatant (S2) obtained after dissolution of the pellet (nano-formulation complexed cell protein), and lane H- $ZnONP_M$.

Sl. No.	Sample	Concentration (µg/mL)
1	Cell lysate	61.3
2	Soluble fraction of αS present in the flocs	46.6
3	Supernatant (obtained after centrifuging incubated flocs and cell lysate)	54.9
4	Pellet (obtained after desorption of bonded cell lysate to the flocs)	21.4
5	Supernatant 2 (obtained after desorption of bonded cell lysate to the flocs)	24.4
6	Flocs after dissolution	31.5
7	$ZnONP_M$	2.9

Table S5: Concentration of protein calculated by BCA assay.

Methodology: For the experiment, SH-SY5Y cell line was used, as the expression of the SNCA gene is relatively lower. Therefore, even the low replacement upon the interaction of the nano-formulation with extracted cell protein can be observed in SDS-PAGE without creating confusion with internal αS expressed in the cell line. Briefly, fully confluent T25 flasks with SH-SY5Y were taken and washed using ice-cold 1X PBS. The adherent cell was scraped and collected in ice-cold RIPA lysis buffer. The obtained cell lysate was further incubated for 30 mins at 4 ^{o}C. The cell lysate was centrifuged at 13000 g for 20 mins at 4 ^{o}C; the supernatant containing the crude cell protein was -20 ^{o}C for further experiment. Further,

the interaction of the crude extract with the flocs was analysed using SDS-PAGE and BCA assay (as per the manufacturers protocol). The flocs (50 μM αS and 30 μg/mL ZnONP complex) were incubated with the cell lysate in 1:1 ratio (v/v) and mixed thoroughly for 24 h at RT. After incubation, the solution was centrifuged at 14000 rpm for 40 mins, and the supernatant and pellet were collected. The pellet containing the bounded cell lysate to the flocs was dissolved in 1x PBS and dissolution of the NP was done. After the dissolution of the np, the sample was further centrifuged, and the supernatant and pellet were collected. The BCA assay and SDS-PAGE were performed for all the samples to get further insights into the flocs and crude cell protein interaction profile.

Results:

As observed in Fig. S15 and Table S5, the total cell proteins exhibited significantly lower affinity towards the NP core as most of the plasma protein was detected in the supernatant fraction of the centrifuged sample (Fig. S15a-lane E and Sl. no. 3 of Table S5). However, a smaller fraction of monomeric αS was also observed in lane E, indicating the replacement of soft corona with the plasma protein (trace amount ~ 40 KDa protein, as recognized in lane F of the silver-stained 10% SDS-PAGE, Fig. S15a). The desorption of the complex further confirmed that ~66% of the monomeric αS retained in the pellet, indicating the slower dissociation rate of hard corona (lane G and Sl. no. 3 of Table S5). In conclusion, αS present in the soft corona will maintain equilibrium with the biological milieu, whereas the monomeric αS sequestered in the hard corona of the NP interface will take a longer duration to be released from the NP core.